Effects of Rib Shapes on Heat Transfer Characteristics of Turbulent Flow of Al₂O₃-Water Nanofluid inside Ribbed Tubes

Mohebbi, Komeil; Rafee, Rohollah*⁺; Talebi, Farhad

Faculty of Mechanical Engineering, Semnan University, P.O. Box 35131-19111 Semnan, I.R. IRAN

ABSTRACT: *In this paper, convection heat transfer of Al₂O₃-water nanofluid turbulent flow through internally ribbed tubes with different rib shapes (rectangular, trapezoidal and semi-circular) is numerically investigated. For each rib shape, the optimum geometric ratio and volume fraction were calculated using entropy generation minimization technique. The governing equations in steady state and axisymmetric form have been solved using Finite Volume Method (FVM) with the SIMPLE algorithm. A uniform heat flux was applied on the wall. A single-phase approach has employed to model the nanofluid. Nanoparticles size is 20 nm and nanoparticles volume fraction and Reynolds number were within the ranges of 0-5% and 10,000-35,000 respectively. Comparisons between the numerical results and experimental data show that among different turbulence models, k-ε model with enhanced wall treatment gives better results. The results indicate that the heat transfer increases with nanoparticles volume fraction and Reynolds number but it is accompanied by increasing pressure drop. The simulations demonstrate that trapezoidal and semi-circular ribbed tubes have higher Nusselt number than the rectangular ribbed tubes with the same diameters. Correlations of heat transfer have obtained for different ribbed tubes. In evaluation of thermal performance and pressure drop, it is seen that the ribbed tubes with Al₂O₃-water nanofluid flow are thermodynamically advantageous. For each rib shape, the optimum geometric ratios are also presented.*

KEY WORDS: *Enhanced heat transfer; Entropy generation; Numerical analysis; Forced convection; Turbulent flow; Ribbed tube.*

INTRODUCTION

Enhancement of heat transfer in engineering applications had been a subject of interest in many research studies. Two different techniques for heat transfer enhancement are generally used; first, fluid additives like nanoparticles are used, second, geometry modification are made by roughening the heat transfer surfaces using ribs, grooves or wires or applying helical corrugated tubes. These modified geometries create the chaotic and good mixing in fluid flow due to the secondary flow regions which appear near the wall and cause to reduce the thickness of thermal boundary layer in a manner that increases the heat transfer rate.

Unfortunately, often by using these techniques for improving the rate of heat transfer, the increase in pressure drop occurs as a penalty [1, 2].

Many researchers have studied the enhancement of heat transfer and pressure drop in rough surfaces experimentally and numerically. Artificial roughness is used in various devices like evaporators, steam condensers, gas turbine blades, cooling channels, nuclear reactors, heat exchangers, and solar air heaters [3-5]. *Donne & Meyer* [6] reported a review of heat transfer coefficient and pressure drop for different rib configurations. *Naphon et al.* [7] conducted an experimental study on the heat transfer and friction factor in horizontal double pipe heat exchanger using helical ribbed tube. They investigated the effect of relative height and pitch of corrugation on the heat transfer and pressure drop and they found that the height of corrugation has more significant effect than the corrugation pitch on the heat transfer and pressure drop. *Kiml et al.* [8] investigated angles of rib (θ=45, 60, 75 and 90) in a ribbed tube under turbulent regime and uniform heat flux condition. Results show that θ =60 is the appropriate angle for heat transfer enhancement and flow circulation. *San & Huang* [9] investigated the heat transfer enhancement of turbulent airflow inside ribbed tube with a length to diameter ratio of 87 under isothermal surface condition, experimentally. The rib pitch to tube diameter ratio (p/d) and the rib height to diameter ratio (e/d) were in the range of 0.304-5.72 and 0.015-0.143, respectively. Their results show that the average of Nusselt number and friction factor were individually correlated as a function of the (p/d) and (e/d). In the many researches, the effectiveness parameter for the heat transfer was examined as a function of the pipe roughness (e/d), Reynolds and Prandtl number. *Bilen et al.* [10] experimentally studied the heat transfer and friction characteristic of a fully developed turbulent airflow in a ribbed tube with different groove shapes (rectangular, trapezoidal and semi-circular) with length to diameter ratio of 33. Results showed that the grooves can enhance the heat transfer up to 63% for circular grooves, 58% for trapezoidal grooves and 47% for rectangular grooves, in comparison with the smooth tube. In addition, they expressed that ribbed tube are thermodynamically advantageous. *Pingan et al.* [11] used standard k-ε turbulent model with enhanced wall treatment

to investigate the heat transfer of the air flow in a channel with different rib shapes (semi-circular, rectangular and triangular) and observed that the average Nusselt number of channel with triangular and rectangular were the largest and smallest, respectively. *Eiamsa-ard et al.* [12] studied the heat transfer in grooved channel with groove-width to channel-height ratio (B/H=0.5-1.75). They found that the grooved channel provides a considerable increase in heat transfer at about 158% with respect to smooth channel and the ratio of B/H=0.75 is obtained as the thermal optimum ratio.

Adding nanoparticles to the base fluid increases the heat transfer due to increasing of the thermal conductivity of nanofluids [13]. Many researchers study this method experimentally and numerically. In general, there are two approaches for simulation of nanofluids: single phase and two phase approach. In the single phase model, it is assumed that the nanoparticles and fluid phase are in hydrodynamics and thermal equilibrium. While two phase model has high accuracy in real, especially in the complicated flow and fluid with big nanoparticles, results have shown that these two approaches have same result approximately when thermo-physical properties are temperature dependent [14]. *Maxwell* [15] on more than 100 years ago studied the mixture of micrometre and millimetre solid particle in the liquids and showed that the conductivity of liquid/solid mixtures raise with particles volume fraction. However, use of them has a high risk of sedimentation and erosion as well as high pressure loss. Compared with suspended particles of micrometre and millimetre dimensions, nanoparticles show very good stability. A nanofluid is a suspension of solid nanoparticle (< 100 nm) in a conventional base fluid. The nanofluids first were proposed by *Choi* [16] in 1995. Next researchers investigated the characteristics and properties of nanofluids. Nanofluids are used in many fields like heat exchangers, automotive industry, aerospace, nuclear reactor, electronic cooling, and refrigeration [17-19]. *Keblinski et al.* [20] introduce four mechanisms that contribute in the increase of nanofluids heat transfer, Brownian motion of the particles, molecular level layering at the liquid/particle interface, nature of nanofluid heat transfer, clusters (high conductivity path). *Das et al.* [21] observed 10-25% increase in thermal conductivity with 1-4% volume fraction of Al_2O_3 nanoparticles in water. Many investigations show that

adding nanoparticles to the base fluids exhibits enhanced thermal conductivity and heat transfer [22-23]. Some researchers have studied the stability of the nanofluids and sedimentation of the nanoparticles in the nanofluids (see e.g., *Jafari et al* [24]). Researchers concluded that the heat transfer enhancement by nanofluids depends on several factors including increment of thermal conductivity, nanoparticles type, size, shape, volume fraction, base fluid and flow regime [25]. *Pak & Cho* [26], *Xuan & Li* [27] and *Maiga et al.* [13] presented three correlations for calculations of the nanofluid Nusselt number in tube as a function of Reynolds and Prandtl numbers in turbulent flows, which show the increase of convective heat transfer coefficient with augmentation of particles volume fraction and Reynolds number.

Duangthongsuk & Wongwise [28] studied the enhancement of heat transfer and pressure drop for Titania-water nanofluid in a double-tube counter flow heat exchanger and showed that the convection heat transfer coefficient and pressure drop of the nanofluid are higher than that of the base fluid. *Fotukian & Nasr Esfahany* [29] studied the heat transfer and pressure drop for small amounts of CuO nanoparticles in water inside a circular tube under turbulent flow regime experimentally and observed that the convective heat transfer coefficient and pressure drop increased by 25% and 20%, respectively.

Recently, some researchers focused on using both method of heat transfer enhancement (i.e. using rough surfaces and nanofluids). For example, *Wongcharee & Eiamsa-ard* [30] experimentally studied the flow of CuO-water nanofluid inside a corrugated tube under turbulent regime. They observed that heat transfer for mentioned geometry with 0.7% volume fraction of CuO increases 1.57 times of that for pure fluid inside the plain tube. *Manca et al.* [31] carried out a numerical investigation on turbulent forced convection of Al_2O_3-water nanofluid in ribbed channel with different rib shapes (square and rectangular). They showed that the heat transfer enhancement increases with the particles volume fraction and Reynolds number but it is accompanied by more pressure drop penalty. *Vatani et al.* [32] numerically investigated the effects of various rib-groove shapes in a horizontal channel for different types of nanofluids on the thermal and hydraulic properties of flow. Their results show that rectangular rib- rectangular groove has the highest performance evaluation criterion and

the SiO_2-water nanofluid provides the highest Nusselt number among all types studied.

As observed, using the ribbed surfaces and adding nanoparticle to base fluid enhance the heat transfer rate and pressure drop. Entropy generation analysis is a ways to optimize a thermal system. Increment of heat transfer reduces the entropy generation but pressure drop augmentation increases entropy generation. Optimum design of thermal system is achieved when the entropy generation is minimized [33]. In the other words, the best design is the case which increases the heat transfer performance with minimum possible pressure drop. Therefore, to determine the optimum design conditions a trade-off between the increase in heat transfer and pressure loss should be done.

It can be realized from above literature review that most of previous investigations focused separately on the effect of the nanofluids flow in smooth tubes for heat transfer enhancement and pressure drop augmentation and very limited data have been reported using nanofluids in other geometries (e.g. in channels) with ribs. In addition, there is not report for method of trade-off between heat transfer enhancement and pressure drop augmentation in nanofluids flow inside ribbed tubes. The optimum rib shape, geometric ratios and volume fractions for nanoparticles have not been obtained for this case. This lack is a motivation for this paper. In this paper, for understanding the effect of the different rib shapes and rib geometry on the heat transfer performance and friction loss, the convective heat transfer of Al_2O_3-water nanofluid in a tube with various rib shapes (rectangular, trapezoidal and semi-circular) and with fixed rib depth at constant wall heat transfer rate is numerically studied. The flow Reynolds number and nanoparticles volume fraction are in the range of 10,000–35,000 and 0–5%, respectively. The entropy generation is used as a criterion for trade-off between heat transfer enhancement and pressure drop augmentation. This criterion is applied to find the optimum rib shape and its geometric ratio. In addition, some correlations for Nusselt number in ribbed tube are presented in this paper. The variations of Nusselt number, friction factor and the entropy generation ratio for different conditions are described in detail.

NUMERICAL METHOD
Problem description

The geometry of the present study is shown in Fig. 1. It consists of a tube with a smooth section of a length
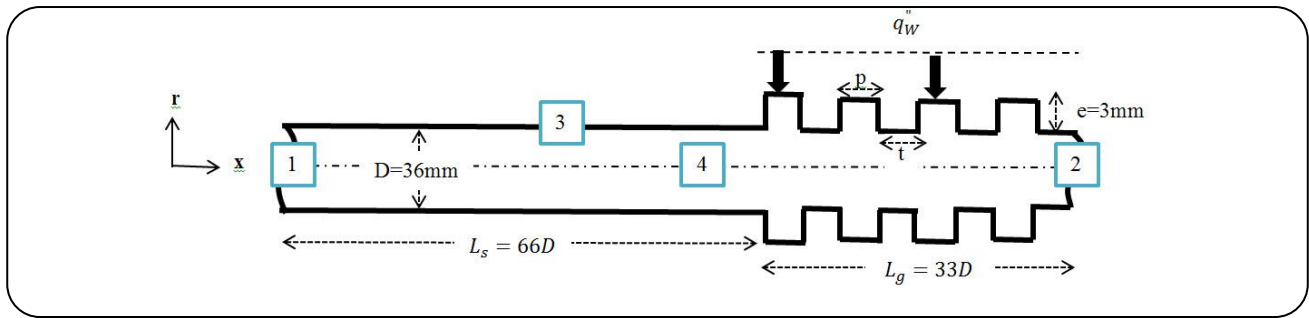
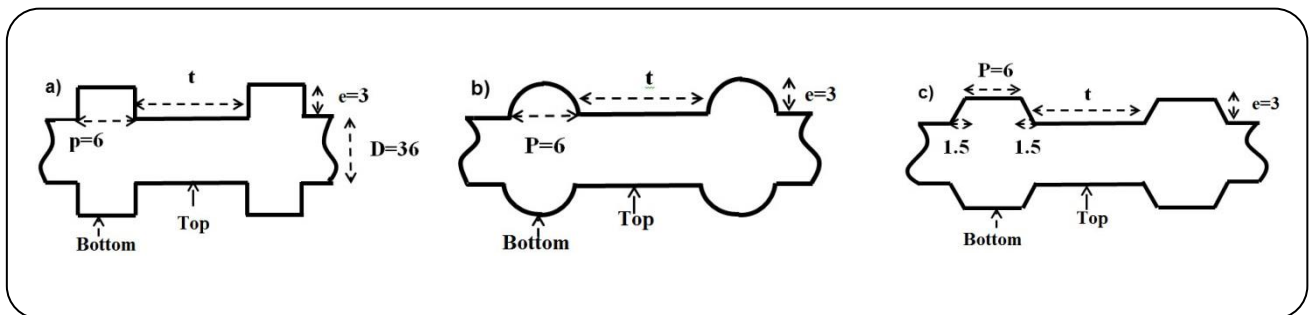*Fig. 1: Geometry of the considered ribbed tube.*

Fig. 2: Details of the ribs shapes (all dimension are in mm) for (a) rectangular, (b) semi-circular, and (c) trapezoidal ribs.

66 D in its entrance to ensure a developed flow and a ribbed section of a length 33 D. The tube diameter is 36 mm and the convection heat transfer inside the tubes with three different rib shapes (rectangular, trapezoidal and semi-circular) and different geometric ratios (0.2 < t/p <2) is investigated. The ribs have a height of e=3 mm and base width of p=6 mm. Both the height and base width are constant. As an example, for the rib ratio of t/p=1, length of the ribs tip is t=6 mm. For this ratio, total number of ribs will be 99 for semi-circular and rectangular ribbed shapes and 79 for trapezoidal ribs (see Fig. 2). A uniform heat flux is applied on tube wall. Uniform flow of Al_2O_3-water nanofluid enters the domain at the inlet section.

Thermo-physical properties of the nanofluids

The thermo-physical properties of Al_2O_3-water nanofluid with a nanoparticles mean diameter of 20 nm are obtained using the assumption of single-phase model.

Calculation of nanofluid density is based on the classical theory of mixture proposed by *Maxwell* [15] which is given by

$$\rho_{nf} = (1-\varphi)\rho_{bf} + \varphi\rho_p \tag{1}$$

Where, ρ_{bf} and ρ_p are the densities of the base fluid and the nanoparticles, respectively.

For specific heat capacity of nanofluid, it is assumed that the base fluid and nanoparticles are in thermal equilibrium. *Xuan & Roetzel* [34] proposed the following equation,

$$c_{p_{nf}} = \frac{(1-\varphi)(\rho c_p)_{bf} + \varphi(\rho c_p)_p}{\rho_{nf}} \tag{2}$$

Where, c_{pbf} and c_{pp} are the specific heat capacity of the base fluid and nanoparticle, respectively.

Viscosity of nanofluid (μ_{nf}) is calculated using the following equation [35],

$$\frac{\mu_{nf}}{\mu_{bf}} = \frac{1}{1 - 34.87\left(\dfrac{d_p}{d_{bf}}\right)^{-0.3}\varphi^{1.03}} \tag{3}$$

In the above equation, d_{bf} is the equivalent molecular diameter of a base fluid, which is given by

$$d_{bf} = 0.1\left[\frac{6M}{N\pi\rho_{f0}}\right]^{\frac{1}{3}} \tag{4}$$

<div align="center">

Table 1: Thermo-physical properties of the materials.

</div>

	ρ (kg/m^3)	C_p (J/kg.K)	k(W/m.K)	μ(kg/m.s)
Water [37]	997.47	4180	0.6	9.45×10^{-4}
Al$_2$O$_3$ (20 nm) [38]	3890	880	36	-

Where *M* is the molecular weight of the base fluid, N is the Avogadro number (6.022×10^{23}, mol^{-1}) and ρ_{f_0} is the density of base fluid at $T_0 = 293$ K.

For evaluating the thermal conductivity of nanofluid (k_{nf}), *Chon et al.* [36] proposed the following equation,

$$\frac{k_{nf}}{k_{bf}} = \tag{5}$$

$$1 + 64.7\varphi^{0.746}\left(\frac{d_{bf}}{d_p}\right)^{0.369}\left(\frac{k_p}{k_{bf}}\right)^{0.7476} Pr^{0.9955} Re^{1.2321}$$

The Prandtl number (Pr), and the Reynolds number (Re) are defined by

$$Pr = \frac{\mu_{bf}}{\rho_{bf}\alpha_{bf}} \tag{6}$$

$$Re = \frac{\rho_{bf} V_{Br} d_p}{\mu} = \frac{\rho_{bf} \kappa_B T}{3\pi\mu^2 l_{bf}} \tag{7}$$

Where α_{bf} is Thermal diffusion coefficient, V_{Br} is the Brownian velocity of nanoparticles, κ_B is the Boltzmann constant (1.3807×10^{-23} J/K), and a constant value of 0.17 nm for the mean free path (l_{bf}) is used for water. The mean free path of the molecule is derived by $d\left(1 l_{bf} = 1/\sqrt{2}n \cdot \pi d_{bf}^2\right)$, where n represents the molecular number. In above equation, the viscosity is expressed by

$$\mu = 2.414 \times 10^{-5} \times 10^{\frac{247}{T-140}} \tag{8}$$

Table 1 shows the thermo-physical properties of water and Al$_2$O$_3$ nanoparticles.

Governing equations

Reynolds averaged Navier Stokes and continuity equations are solved in the axisymmetric form for a turbulent, two-dimensional, steady state, and incompressible flow [39, 40].

Continuity equation:

$$\frac{1}{r}\frac{\partial(rV_r)}{\partial r} + \frac{\partial V_x}{\partial x} = 0 \tag{9}$$

Momentum equations:

$$V_r\frac{\partial V_x}{\partial r} + V_x\frac{\partial V_x}{\partial x} = \tag{10}$$

$$-\frac{1}{\rho}\frac{\partial p}{\partial x} + \frac{1}{\rho}\left[\frac{1}{r}\frac{\partial}{\partial r}\left(r(\mu+\mu_t)\frac{\partial V_x}{\partial r}\right) + \frac{\partial}{\partial x}\left((\mu+\mu_t)\frac{\partial V_x}{\partial x}\right)\right]$$

$$V_r\frac{\partial V_r}{\partial r} + V_x\frac{\partial V_r}{\partial x} = -\frac{1}{\rho}\frac{\partial p}{\partial r} + \frac{1}{\rho}\times \tag{11}$$

$$\left[\frac{1}{r}\frac{\partial}{\partial r}\left(r(\mu+\mu_t)\frac{\partial V_r}{\partial r}\right) + \frac{\partial}{\partial x}\left((\mu+\mu_t)\frac{\partial V_r}{\partial x}\right) - \frac{V_r}{r^2}(\mu+\mu_t)\right]$$

Energy equation:

$$V_x\frac{\partial T}{\partial x} + V_r\frac{\partial T}{\partial r} = \tag{12}$$

$$\frac{1}{\rho c_p}\left[\frac{1}{r}\frac{\partial}{\partial r}\left(r(k+k_t)\frac{\partial T}{\partial r}\right) + \frac{\partial}{\partial x}\left((k+k_t)\frac{\partial T}{\partial x}\right)\right]$$

Where μ_t and k_t are turbulent viscosity and conductivity those after simplifying the Equations (10-12) using Reynolds average approach and given as:

$$k_t = \frac{c_p\mu_t}{\sigma_t} \tag{13}$$

$$\mu_t = C_\mu\rho\frac{k^2}{\varepsilon} \tag{14}$$

μ_t needs to be modelled. As an example, the k- ε turbulence model with following transport equations is used for calculation of the turbulent viscosity. In the k-ε turbulence model, the turbulent kinetic energy (*k*) is calculated by solving the following transport equation,

$$\frac{1}{r}V_r\frac{\partial(rk)}{\partial r} + V_x\frac{\partial(k)}{\partial x} = \tag{15}$$

$$\frac{1}{\rho}\left[\frac{1}{r}\frac{\partial}{\partial r}\left(r\left(\mu+\frac{\mu_t}{\sigma_k}\right)\frac{\partial k}{\partial r}\right) + \frac{\partial}{\partial x}\left(\left(\mu+\frac{\mu_t}{\sigma_k}\right)\frac{\partial k}{\partial x}\right)\right] + G_k - \rho\varepsilon$$

Table 2: Constants in the k-ε turbulence model transport equations.

σ_t	σ_k	σ_ε	$C_{1\varepsilon}$	$C_{2\varepsilon}$	C_μ
0.85	1	1.3	1.44	1.92	0.09

And the transport equation for turbulent dissipation rate (ε) is,

$$\frac{1}{r} V_r \frac{\partial(r\varepsilon)}{\partial r} + V_x \frac{\partial(\varepsilon)}{\partial x} = \tag{16}$$

$$\frac{1}{\rho}\left[\frac{1}{r}\frac{\partial}{\partial r}\left(r\left(\mu+\frac{\mu_t}{\sigma_\varepsilon}\right)\frac{\partial\varepsilon}{\partial r}\right)+\frac{\partial}{\partial x}\left(\left(\mu+\frac{\mu_t}{\sigma_\varepsilon}\right)\frac{\partial\varepsilon}{\partial x}\right)\right]+$$

$$C_{1\varepsilon}\frac{\varepsilon}{k}G_k - C_{2\varepsilon}\rho\frac{\varepsilon^2}{k}$$

Where G_k the rate of production of turbulent kinetic and $\rho\varepsilon$ is its destruction rate, which G_k is given by:

$$G_k = \mu_t\left|\nabla V + \nabla V^T\right|^2 \tag{17}$$

σ_k and σ_ε are turbulent Prandtl number for turbulent kinetic energy and turbulent dissipation rate, respectively. Also C_μ, $C_{1\varepsilon}$ and $C_{2\varepsilon}$ are constant. The model constants are listed in Table 2.

Enhanced wall-treatment method is used in this study because its results are more accurate near the wall.

At the inlet, the values of k and ε are calculated using turbulence intensity (I) which is calculated using the following equation.

$$I = 0.16 Re^{-1/8} \tag{18}$$

In addition, for calculation of the entropy generation, the second law of thermodynamics for a control volume system is used. Here the entire solution domain is considered as a control volume and required surface integrals are calculated using the numerical simulation results. The entropy generation is given by the following equation.

$$\dot{S}_{gen} = \dot{m}_{out}S_{out} - \dot{m}_{in}S_{in} - \int\frac{q''}{T}dA \tag{19}$$

The dimensionless parameters that are used in this study, are the Reynolds number (*Re*), average Nusselt number $\left(\overline{Nu}\right)$, flow friction factor (*f*) and entropy generation ratio (*Ns,a*) which are given by the following relations.

$$Re = \frac{\rho_{nf} V_{avg} D}{\mu_{nf}} \tag{20}$$

$$\overline{Nu} = \frac{\bar{h}\cdot D}{k_{nf}} = \frac{q''}{\left(\overline{T_w}-\overline{T_b}\right)}\cdot\frac{D}{k_{nf}} \tag{21}$$

Where, q'' is heat flux. $\overline{T}_w$ and $\overline{T}_b$ represent the average temperature of the wall and bulk flow temperature, respectively. Friction factor of the flow is determined by

$$f = \frac{2(\Delta p)}{\left(\dfrac{L}{D}\right)\cdot\rho_{nf}\cdot V_{avg}^2} \tag{22}$$

Where, *L* is the pipe length.

The entropy generation ratio is used as a criterion for evaluation of the thermal performance of the system. This parameter is defined by

$$N_{s,a} = \frac{\dot{S}'_{gen,a}}{\dot{S}'_{gen,0}} \tag{23}$$

Where $\dot{S}'_{gen,a}$ represents the entropy generation rate per length of the test section (nanofluid flow inside a ribbed tube) and $\dot{S}'_{gen,0}$ represents entropy generation rate per length in reference conditions (base fluid flow inside a smooth tube with the same length) [33]. According to Eq. (23), the system will be thermodynamically advantageous if $N_{s,a}$ values are less than 1.

Boundary conditions

Above equations are solved using the following boundary conditions (see Fig. 1).

1) Uniform inlet Velocity

$$V_x = V_{in} \ , \ V_r = 0 \ \text{and} \ T_{in} = 295.13\,K \tag{24}$$

Table 3: Grid independence test results.

Geometry	Mesh Type	Number of cells	Changes in Average Nu (%)
Smooth tube	Structured	400,000 600,000	0.02
Rectangular ribs	Unstructured	1,430,094 2,298,108 2,556,567	4.4 0.02
Rectangular ribs	Structured	1,400,000 1,600,000 1,800,000	0.15 0.07
Trapezoidal ribs	Structured	825,000 1,194,300 1,400,000	0.92 0.67
Semi-circular ribs	Structured	1,315,323 1,500,000	1.9
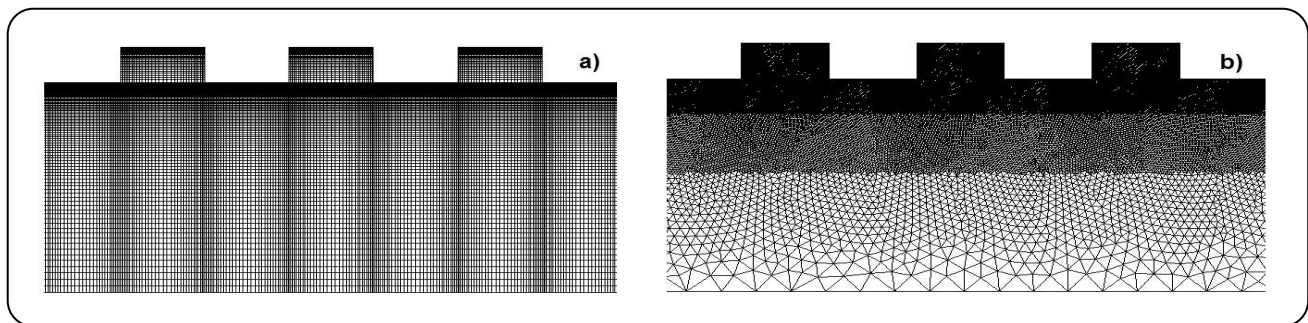
Fig. 3: Meshes for ribbed tube a) structured b) unstructured mesh.

2) Zero gradient for velocity components at outlet

$$\frac{\partial}{\partial x}\left(V_x\right) = 0 \quad , \quad \frac{\partial}{\partial x}\left(V_r\right) = 0 \tag{25}$$

3) Wall boundary conditions

$$V_x = 0 \quad , \quad V_r = 0 \quad \text{and} \quad -k_{eff} \cdot \frac{\partial T}{\partial n}\bigg|_{wall} = q'' \tag{26}$$

4) Axisymmetric condition

$$\frac{\partial}{\partial \theta}\left(V_x\right) = 0 \quad , \quad \frac{\partial}{\partial \theta}\left(V_r\right) = 0 \quad \text{and} \quad \frac{\partial}{\partial \theta}\left(T\right) = 0 \tag{27}$$

Numerical procedure

The governing equations (eqs. (9) to (12)) were discretized using finite volume method. The SIMPLE algorithm is used for pressure velocity coupling (See *Rafee & Rahimzadeh* [40]). The second order upwind scheme has used to discretize the momentum, turbulent kinetic energy, turbulent dissipation rate, and energy equations. The iterative procedure is terminated when the residual values are lower than 10^{-5}.

For checking the grid independence of the solution, several structured and unstructured meshes were generated. As an example, the structured and unstructured meshes for rectangular ribbed tube are shown in Fig. 3. The average Nusselt number is used for comparing the results of different meshes. The obtained results are listed in Table 3.

As can be seen, the appropriate number of cells in terms of accuracy and solution time for smooth tube and ribbed tube (with rectangular, trapezoidal and semi-circular ribbed shape and all in ratio t/p=1) are 400,000 1,400,000 1,194,300 and 1,315,323, respectively.

In order to demonstrate the validity and precision of the turbulence models and numerical procedure,
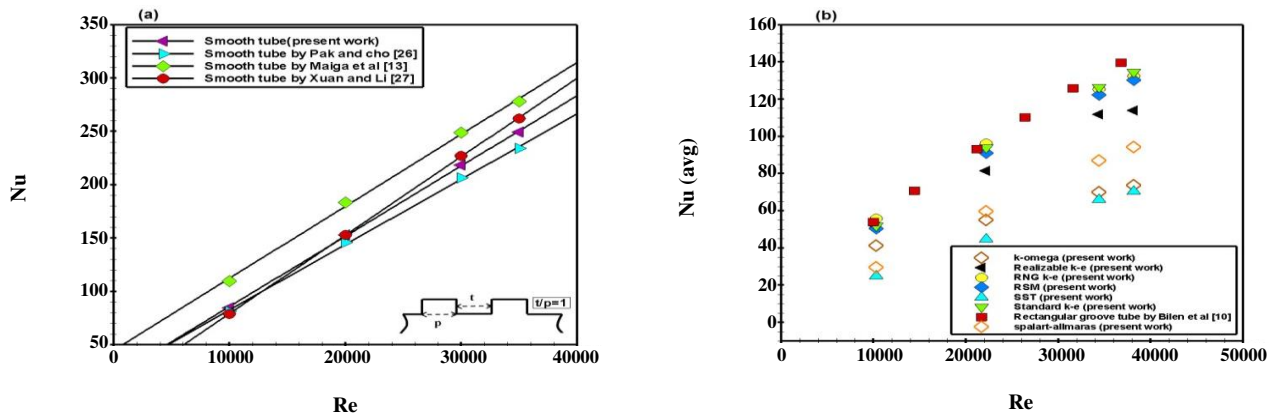
Fig. 4: Comparison between predicted average Nusselt number a) and available correlation for Al₂O₃-water nanofluid in smooth tube, (b) and experimental data of Bilen et al. [10] for airflow in ribbed tube (t/p=1).

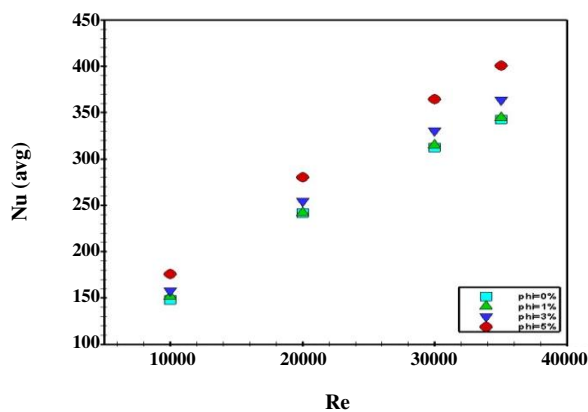*Fig. 5: The influence of the Al₂O₃ nanoparticles volume fraction on the average Nusselt number for different Reynolds numbers of the flow in the ribbed tube (rectangular ribs with geometric ratio of t/p=1).*

the variations of average Nusselt number with the flow Reynolds number for smooth and ribbed tubes are compared in Fig. 4. Firstly, the results obtained in a smooth tube are compared with correlations of *Pak & Cho* [26], *Xuan & Li* [27] and *Maiga et al.* [13] for Al₂O₃-water nanofluid.

Fig. 4 (a) shows good agreement between results of present work and those obtained from the correlations for Al₂O₃-water nanofluid flow in smooth tube. The difference between the obtained results and correlations of *Xuan & Li*, *Pak & Cho* and *Maiga et al.* are 4, 5, and 18%, respectively. The results of ribbed tube (Fig. 4(b)) with t/p=1 are compared with experimental data of *Billen et al.* [10] for airflow. Among different turbulence models, Standard k-ε, RNG k-ε with enhancement wall

treatment and RSM model yield the better predictions with maximum deviations of 6, 8 and 9%, respectively. Therefore, the Standard k-ε model with enhancement wall treatment has been chosen for the simulations.

RESULTS AND DISCUSSION

The simulation of convective heat transfer of Al₂O₃-water nanofluid flow are performed for nanoparticles volume fractions in the range of φ=0 to 5% and constant heat rate of Q=10,000 Watts at tube walls of different ribbed and smooth tubes.

Fig. 5 displays the effect of Al₂O₃ nanoparticles volume fraction on the average Nusselt number in a tube with rectangular ribs with geometric ratio of t/p=1. The results indicate that by increasing the nanoparticles volume fraction and flow Reynolds number, the average Nusselt number will enhance. For nanoparticles volume fraction of 3%, the average Nusselt number has increased by 6% at Reynolds number of 30,000.

Adding nanoparticles has an adverse effect on the viscosity of the nanofluid and causes more pressure drop. Fig. 6 indicates the ratio of pressure drop of nanofluid to that of the base fluid for different Reynolds numbers and nanoparticles volume fractions. Applying volume fractions of 3% for nanoparticles will double the pressure drop.

Using nanofluids can increase the pumping power significantly. The pumping power is defined by

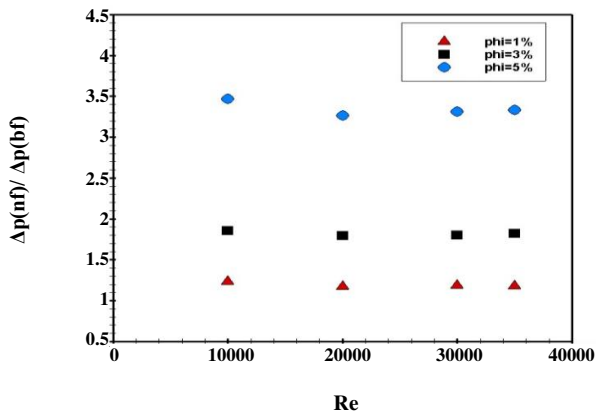$$\text{Pumping power} = \Delta P \cdot Q = \frac{\dot{m} \cdot \Delta P}{\rho_{nf}} \qquad (28)$$

Fig. 6: The influence of nanoparticles volume fraction on the flow pressure drop ratio in the ribbed tube (rectangular ribs with geometric ratio of t/p=1).
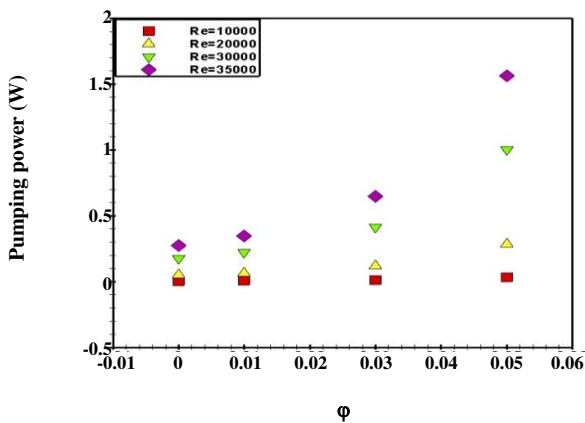

Fig. 7: Variations of the required pumping power with nanoparticles volume fraction in the ribbed tube (rectangular ribs with geometric ratio of t/p=1).
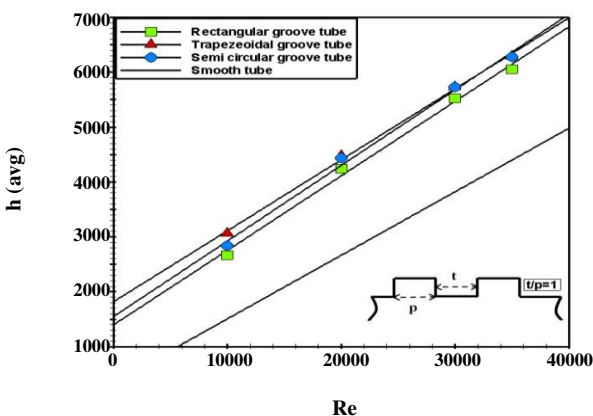

Fig. 8: Variations of average convection heat transfer coefficient with flow Reynolds number for ribbed and smooth tubes (φ=0.01 and t/p=1).

Where, ΔP is the pressure drop and Q is the volumetric flow rate of the nanofluid.

As depicted in Fig. 7, the pumping power increases with the nanoparticles volume fraction. There is a significant increase in pumping power when using the nanofluid compared with the base fluid, especially for higher Reynolds numbers. This implies that the nanofluids need additional pumping power.

Fig. 8 displays the influence of different rib shapes on the average of heat transfer coefficient. The results are presented for nanoparticles volume fraction of φ=0.01. Fig. 8 indicates that for flow Reynolds number of Re=20,000 by using different rib shapes with geometric ratio of t/p=1, the average convection heat transfer coefficient enhancement of 66% for trapezoidal ribs, 65% for semi-circular ribs and 58% for rectangular ribbed tube will be obtained in comparison with the smooth tube. This is due to greater production of turbulence, increase in the heat transfer area, and more flow mixing in the ribbed tube. In addition, existence of the ribs provides periodic redevelopment of the boundary layers over their tip, which causes a more effective heat transfer.

In addition, it can be said that more increase in the heat transfer augmentation for trapezoidal and semi-circular ribbed tube is due to the fact that the flow mixing and sweeping surface in these types of ribs are more than those of the rectangular ribs. The recirculation region of the flow inside these types of ribs is smaller than that of the rectangular ribs. One can conclude that the flow mixing and disturbances for the trapezoidal ribs were more than that for the circular ribs.

In Fig. 9. the Nusselt number for the flows with Reynolds numbers in the range of 10,000–35,000 inside the ribbed tubes (t/p=1) are compared with results of correlations presented by *Prandtl* [41], *Petukhove* [42], and *Gnielinski* [43]. The mentioned correlations are as follows.

$$\frac{Nu}{Re\,Pr} = \frac{f/8}{1+8.7\left(f/8\right)^{1/2}\left(Pr-1\right)} \tag{29}$$

$$\frac{Nu}{Re\,Pr} = \frac{f/8}{1.07+12.7\left(f/8\right)^{1/2}\left(Pr^{2/3}-1\right)} \tag{30}$$

$$Nu = \frac{\left(f/8\right)\left(Re-1000\right)Pr}{1+12.7\left(f/8\right)^{0.5}\left(Pr^{2/3}-1\right)} \tag{31}$$

The figure shows that results obtained from present work for ribbed tubes are in good agreement with result obtained by Prandtl formula but the results of *Gnielinski & Petukhove* formulas are greater than that of the present work.

Variations of local convection heat transfer coefficient at the ribbed tube walls (for different shapes and constant geometric ratio of t/p=1) is compared with that of the smooth tube for Re=20,000 and φ=0.03 in Fig. 10. As can be seen, the obtained function of h(x) for smooth tube has a decreasing trend. For ribbed tubes, the variations of the heat transfer coefficient is quite complex. At the base of the ribs a dead zone form and the heat transfer coefficient is law due to lower velocity of the flow. When the flow reaches the tip of the ribs, maximum local heat transfer coefficient occurs. Here the variations of the heat transfer coefficient are similar to that of a boundary layer flow over a flat plate. These variations repeat periodically but with reduced amplitude.

In Fig. 11 friction factor changes with flow Reynolds number for different ribbed tubes with the geometry ratios of t/p=1 and t/p=0.5 are compared with those of the smooth tube. The friction factor has a decreasing trend. In addition, the friction factor of the ribbed tube is higher than that of the smooth tube. For example, at Reynolds number of 20,000, the friction factor of the tube with trapezoidal ribs is 4 times the friction factor of smooth tube and the tubes with rectangular and semi-circular ribs have a friction factor that is about 3 times the friction factor of smooth tube. The mentioned results are obtained for the ribs with geometric ratios of t/p=1. For geometric ratio of t/p=0.5, friction factor of the tubes with trapezoidal ribs is about five times the friction factor of smooth tube. On the other hand, for rectangular and semi-circular ribs, the friction factor of the flow is 4 times the friction factor of smooth tube.

Due to the increasing of rib area in trapezoidal rib, friction factor of trapezoidal rib tube is more than the friction factor of other ribbed tubes.

The equivalent relative roughness (ε / D) for ratios of t/p=1 and t/p=0.5 are given in Table 4. It is evident that for higher ratios of t/p, the distances between the ribs are less. It should be noted that the values of relative roughness are obtained by comparing the predicted values of friction factor (which is calculated by Eq. 22) and
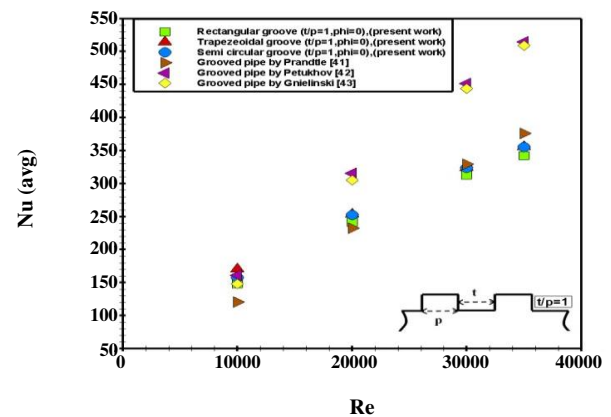

Fig. 9: Comparison between the result of present work and available correlations for average Nusselt number of the water flow inside the ribbed tubes with t/p=1.
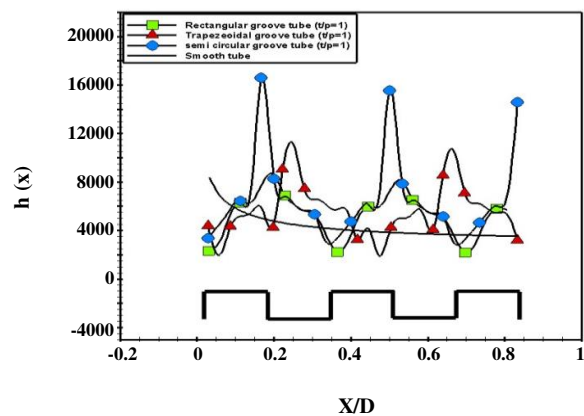

Fig. 10: Comparison between local heat transfer coefficient (in W/m²K) for different rib shapes (t/p=1, φ=0.01, and Re=20,000) and the smooth tube.
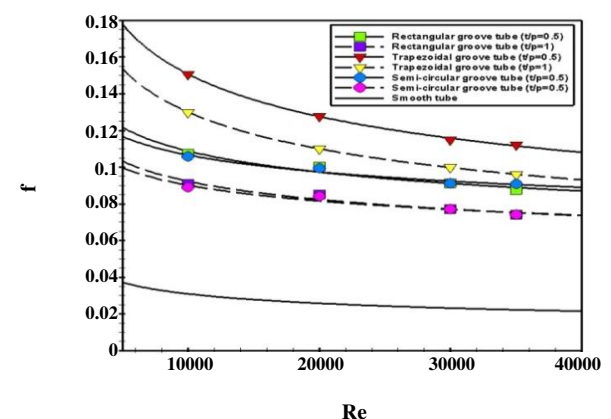

Fig. 11: Predicted friction factors for ribbed and smooth tubes versus the flow Reynolds number.

Table 4: Equivalent relative roughness (ε / D) for ribbed tubes.

Rib type	$\left.\dfrac{\varepsilon}{D}\right|_{t/p=1}$	$\left.\dfrac{\varepsilon}{D}\right|_{t/p=0.5}$
rectangular	0.066	0.091
trapezoidal	0.113	0.146
Semi-circular	0.065	0.091

Table 5: Proposed correlations for calculation of the nanofluid heat transfer Nusselt number in smooth and ribbed tubes.

geometry	formula	
Smooth tube	$\overline{Nu} = 0.02\,Re^{0.8264}\,Pr^{0.4019}$	
	t/p=1	t/p=0.5
Rectangular tube	$\overline{Nu} = 0.2076\,Re^{0.6421}\,Pr^{0.3763}$	$\overline{Nu} = 0.3255\,Re^{0.5806}\,Pr^{0.5244}$
Trapezoidal rib tube	$\overline{Nu} = 0.6109\,Re^{0.5216}\,Pr^{0.4716}$	$\overline{Nu} = 1.286\,Re^{0.6047}\,Pr^{-0.3194}$
Semi-circular rib tube	$\overline{Nu} = 0.2856\,Re^{0.6101}\,Pr^{0.3987}$	$\overline{Nu} = 0.6229\,Re^{0.5919}\,Pr^{0.139}$

the explicit formula proposed by *Haaland* [44]. The mentioned equation is

$$f^{-1/2} = -1.8\log(\frac{6.9}{Re} + (\frac{\varepsilon / d}{3.7})^{1.11}) \qquad (32)$$

Using the obtained data of the present work, different correlations are proposed here for calculation of the average Nusselt numbers of the Al_2O_3-water nanofluid heat transfer. The proposed correlations are given in Table 5.

The maximum deviations of the calculated average Nusselt numbers by above correlations from the numerical results are 0.48% for smooth tube and 0.72%, 0.17 and 0.68% for rectangular, trapezoidal and semi-circular ribs, respectively (for ribs with geometric ratio of t/p=1). Also, the deviations for tubes with rectangular, trapezoidal and semi-circular ribbed tubes with t/p=0.5 are 0.56%, 2.1% and 0.24%, respectively. The results of the correlations for average Nusselt number are plotted against the numerical results of the simulations in Fig. 12.

Fig. 13 shows the influences of changing the rib geometric ratio (t/p) on average Nusselt number for ribbed tubes at Re=10,000. The results indicate that lower values of t/p can increase the average Nusselt number. The highest values of average Nusselt number occurs at t/p=0.2 for rectangular and semi-circular ribbed tube and at t/p=0.25 for trapezoidal ribbed tube.

Fig. 14 depicts the flow pattern and recirculation zone for different ribs at Re=20,000 and $\varphi = 0.03$. In the figure, the fluid temperature is high near the walls and the core region is poorly influenced. Also for trapezoidal and semi-circular ribbed tube, the mixing is stronger and the differences between the bulk flow and wall temperatures decrease so the heat transfer mechanism becomes more efficient.

The flow patterns near the ribs for different values of t/p are shown in Fig. 15. For smaller values of t/p, there are more spaces for flow mixing. This flow mixing increases the heat transfer coefficients and friction factors.

For different rib shapes, variations of friction factor with the geometric ratios of t/p are shown in Fig. 16. The highest values of friction factor is obtained at geometric ratio of t/p=0.2 for semi-circular and rectangular ribbed tube and the ratio of t/p=0.25 for trapezoidal ribbed tube.
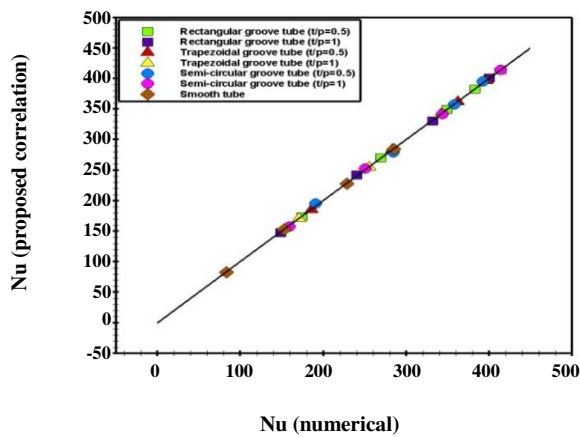
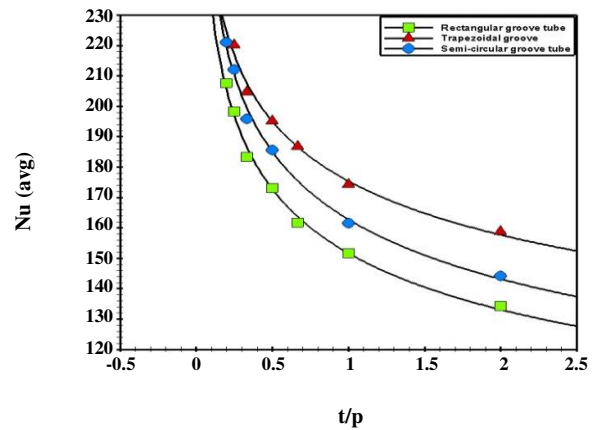**Fig. 12: predicted values for Nusselt number versus the results of the proposed correlations.**

Fig. 13: Average Nusselt number as a function of the geometric ratio of the rib (t/p) on Re=10,000 and φ=0.01 for ribbed tubes with different geometric rib shapes.
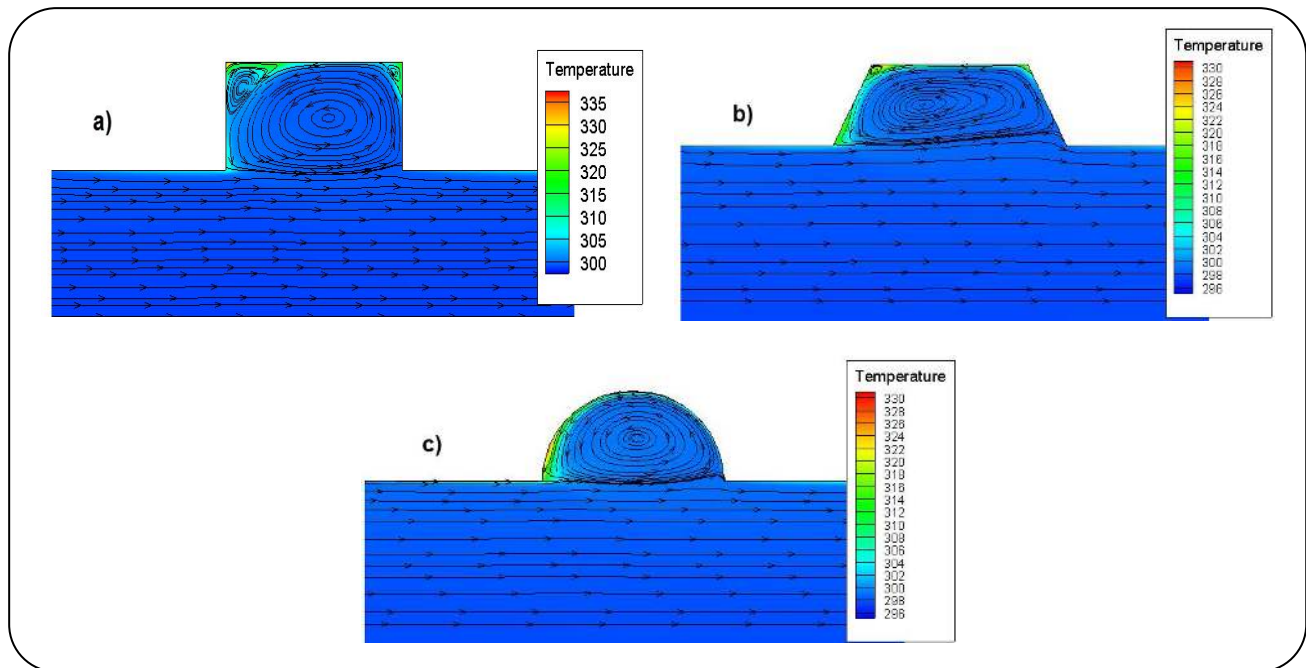

Figure 14: Temperature contours (in K) and streamlines near the base of the ribs for (a) rectangular, (b) trapezoidal and (c) semi-circular ribbed tubes with t/p=1 (Re=20,000 and φ=0.03).

From above discussion, it is evident that adding nanoparticles and ribs can enhance the convection heat transfer coefficients but both of them increase the pressure drop. Here the irreversibility of the heat transfer is used as a criterion for evaluation of both parameters. For this purpose, the entropy generation ratio ($N_{s,a}$) is used (See Eq. (23)).

Fig. 17 shows the effects of rib geometric ratio (t/p) on entropy generation ratio. The flow Reynolds number is

10,000 and nanoparticles volume fraction of φ=0.01 is considered for these simulations. It is seen from the figure that at all geometric ratios (t/p), the ribbed tubes are thermodynamically advantageous ($N_{s,a}$<1), because of reduced irreversibility of heat transfer process overcomes the negative effects of the pressure drop. These results also indicate that the minimum entropy generation ratio occurs at the geometric ratio of t/p=0.25 for semi-circular and rectangular ribs and at the geometric ratio of t/p=0.33
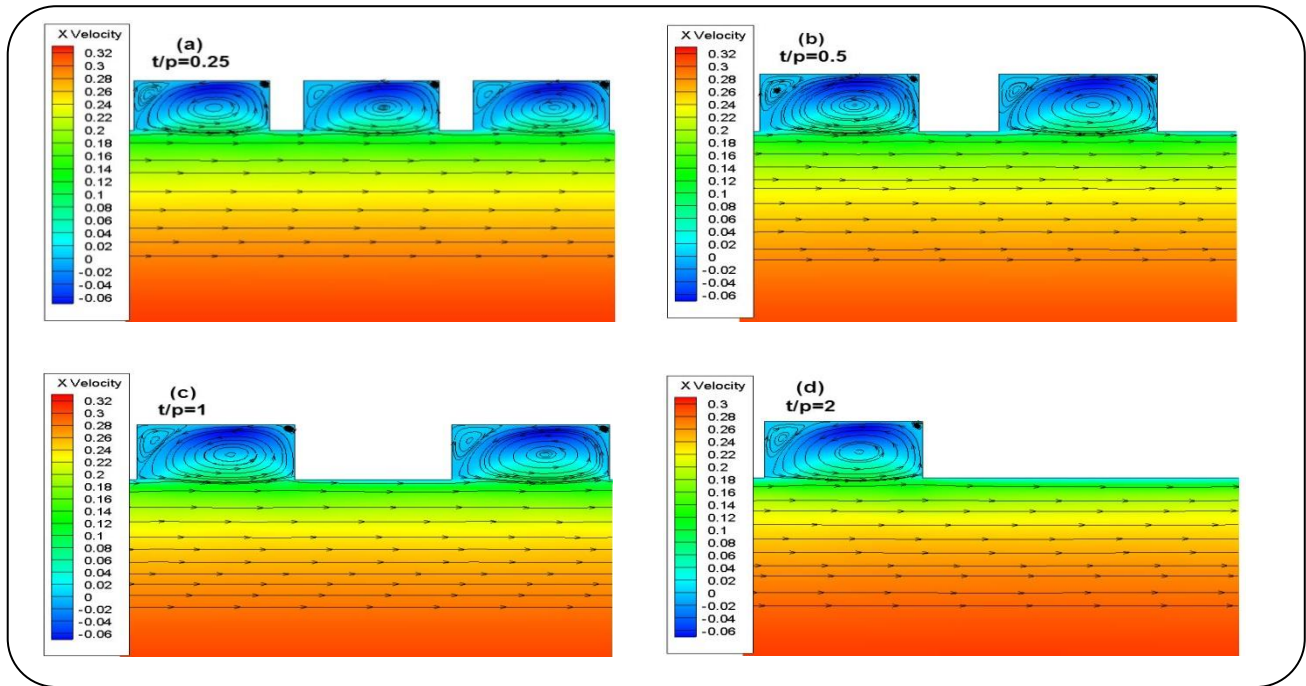
Fig. 15: Flow patterns (velocities are in m/s) near the rectangular ribs for different values of t/p (φ=0.01, Re=10000).
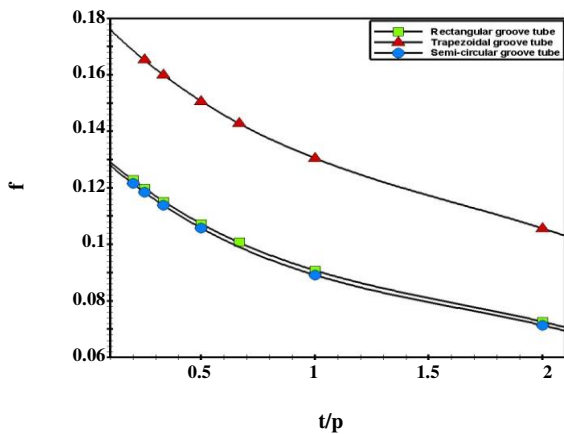

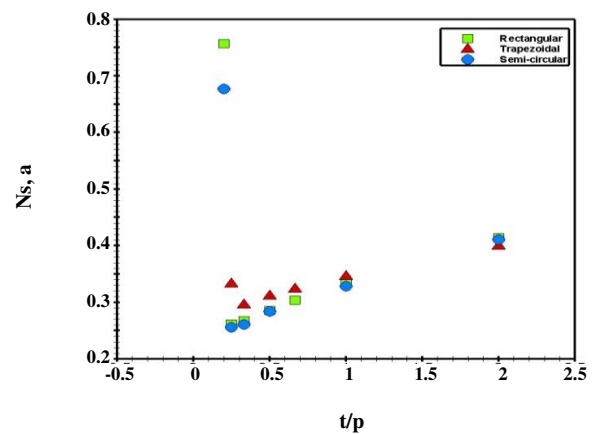*Fig. 16: The effects of geometric ratio (t/p) on friction factor for different rib shapes at Re=10,000.*

Fig. 17: Variations of the entropy generation ratio with geometric ratio for ribbed tubes (t/p) (Re=10000, φ=0.01).

for trapezoidal ribs. The semi-circular ribs are thermodynamically advantages and ratio of t/p=0.25 gives the optimum condition.

To study the effects of adding nanoparticles and Reynolds number flow, in Fig. 18 shows the entropy generation ratio of water-Al_2O_3 flow versus volume fraction of the nanoparticles at different flow Reynolds numbers in a tube with semi-circular ribs at the ratio of t/p=0.25. It is shown that the entropy generation ratio has

a linear decreasing trend by adding nanoparticles and increasing the flow Reynolds number results in better thermal performance when the nanofluids and ribs are applied simultaneously. This figure demonstrates that the entropy generation ratio will decrease about 40% by adding 5% of nanoparticle at Re=35,000. It can be concluded that the best thermal condition can be obtained for flow with Reynolds number of 35,000 and nanoparticles volume fraction of 0.05.
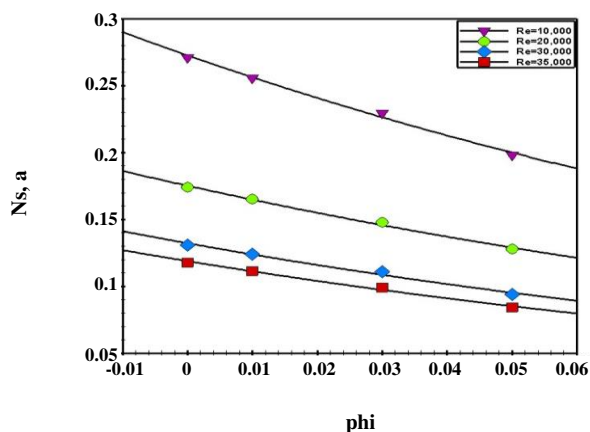
Fig. 18: The effects of nanoparticles volume fraction (φ) and the flow Reynolds number on the entropy generation ratio for optimum rib shape and geometric ratio (semi-circular ribs with t/p=0.25).

CONCLUSIONS

In this study, the heat transfer characteristics of the turbulent forced flows of Al_2O_3-water nanofluid at different Reynolds numbers and nanoparticles volume fractions, flowing inside a ribbed tube with different rib shapes and at different geometric ratios (t/p) of ribs were investigated numerically. Constant wall heat flux condition was applied which results in constant heat rate of Q=10,000 Watts for all simulations.

Comparison between the predicted results of the different turbulence models and available experimental data show that standard k-ε and RNG k-ε models with enhancement wall treatment are more suitable for simulations of the nanofluid flow and heat transfer in the ribbed tubes. Average heat transfer coefficient enhancement is up to 66% for trapezoidal rib, 65% for semi-circular ribbed and 58% for rectangular ribbed tube with geometric ratio of t/p=1, in comparison with the smooth tube at Re=20,000.

The friction factor of the ribbed tube is higher than that of the smooth tube. Friction factor of the tubes with trapezoidal ribs is 4 times the friction factor of the smooth tube and friction factors for rectangular and semi-circular are 3 times the friction factor of smooth tube at a Reynolds number of 20,000 (at the geometric ratio of t/p=1). It was shown that for smaller values of the t/p the flow mixing occurs more times. This flow mixing increases the heat transfer coefficient and flow friction factor. The highest values of the average Nusselt number

and friction factor occurs at t/p=0.2 for semi-circular and rectangular ribs and at the ratio of t/p=0.25 for trapezoidal ribs.

A significant increase in the pumping power and pressure drop is observed when nanofluid is used, especially at the higher Reynolds number, that it is the disadvantage of using the nanofluids. Ribbed tubes are thermodynamically advantageous. The results indicate that the entropy generation ratio is minimized for tubes with semi-circular and rectangular ribs at the geometric ratio of t/p=0.25. For trapezoidal ribs, the ratio of t/p=0.33 gives minimum entropy generation number. These ratios can be selected as the optimum value from the thermodynamic point of view.

Nomenclature

t	Ribs Tip width, mm
p	Ribs Tip width, mm
k	Turbulent kinetic energy, m^2/s^2
ε	Turbulent dissipation rate, m^2/s^2
θ	Degree, °C
D	Diameter, mm
e	Equivalent roughness height, mm
Nu	Nusselt number $=hD/k$
φ	Nanoparticles volume fraction
Re	Reynolds number $=\rho VD/\mu$
Pr	Prandtl number $=\upsilon/\alpha$
Pe	Peclet number $=u.d/\alpha$
n	Number of the ribs
σ_k	Turbulent Prandtl number for k
σ_ε	Turbulent Prandtl number for ε
I	Turbulent intensity
$\dot{m}$	Mass flow rate, kg/s
A	Area, m^2
$\dot{S}'$	Rate of entropy per unit length (W/mK)
f	Friction factor
$N_{s,a}$	Entropy generation ratio $= \left(\dot{S}'_{gen,a} / \dot{S}'_{gen,0} \right)$
L	Length, m
h	Convective heat transfer coefficient, $W/m^2\,K$
Q	Heat transfer rate, W
ρ	Density, kg/m^3
c_p	Specific heat capacity, J/kg.K
μ	Viscosity, $N.s/m^2$
M	Molecular weight, g/mol
N	Avogadro constant $=6.022 \times 10^{23}$ (mol^{-1})

T	Temperature, K
k	Thermal conductivity, W/m.K
α	Thermal distribution, m^2/s
V	Velocity, m/s
κ_B	Stefan-Boltzmann constant = 1.3807×10^{-23}(J/K)
l_{bf}	Mean free path, nm
P	Pressure, Pa
σ_t	Turbulent Prandtl number

Subscripts

nf	Nanofluid
s	Smooth
g	Rib
bf	Base fluid
p	Particle
Br	Brownian
t	Turbulence
gen	Generation
a	Augmented
0	Reference conditions
w	Wall

REFERENCES

[1] Rafee R., Entropy Generation Calculation for Laminar Fully Developed Forced Flow and Heat Transfer of Nanofluids Inside Annuli, *J. Heat Mass Trans. Res.*, **1**; 25-33 (2014).

[2] Duangthongsuk W., Wongwises S., An Experimental Study on the Heat Transfer Performance and Pressure Drop of TiO$_2$-Water Nanofluids Flowing under a Turbulent Flow Regime, *Int. J. Heat Mass Trans.*, **53**:334–44 (2010).

[3] Durga Prasad P.V., Gupta A.V.S.S.K.S., Sreeramulu M. , SyamSundar L., Singh M.K., Antonio C.M. Sousa, Experimental Study of Heat Transfer and Friction Factor of Al$_2$O$_3$ Nanofluid in U-Tube Heat Exchanger with Helical Tape Inserts, Exp. *Therm. Fluid Sci.*, **62**: 141-150 (2015).

[4] Ji W.T., Zhang D.C., He Y.L., Tao W.Q., Prediction of Fully Developed Turbulent Heat Transfer of Internal Helically Ribbed Tubes - An Extension of Gnielinski Equation, *Int. J. Heat Mass Trans.*, **55**(4): 1375-1384 (2012).

[5] Li Zh., Lu J., Tang G., Liu Q., Effects of Rib Geometries and Property Variations on Heat Transfer to Supercritical Water in Internally Ribbed Tubes, *Appl. Therm. Eng.*, **78**:303-314 (2015).

[6] Dalle Donne M., Meyer L., Turbulent Convective Heat Transfer from Rough Surfaces with Two-Dimensional Rectangular Ribs, *Int. J. Heat Mass Trans.*, **20**:583-620 (1977).

[7] Naphon P., Nuchjapo M., Kurujareon J., Tube Side Heat Transfer Coefficient and Friction Factor Characteristics of Horizontal Tubes with Helical Rib, *Energy Convers. Manage*, **47**: 3031-3044 (2006).

[8] Kiml R., Magda A., Mochizuki S., Murata A., Rib-Induced Secondary Flow Effects on Local Circumferential Heat Transfer Distribution Inside a Circular Rib Roughened Tube, *Int. J. Heat Mass Transfer*, **47** (6–7): 403-412 (2004).

[9] San J.Y., Huang W.C., Heat Transfer Enhancement of Transverse Ribs in Circular Tubes with Consideration of Entrance Effect, *Int. J. Heat Mass Trans.*, **49** (17-18): 2965-2971 (2006).

[10] Bilen K., Cetin M., Gul H., Balta T., The Investigation of Groove Geometry Effect on Heat Transfer for Internally Grooved Tubes, *Appl. Therm. Eng.*, **29**: 753-761 (2009).

[11] Pingan L., Ye G., Hairong M., Liu H., Numerical Simulation of Heat Transfer and Resistance Pattern in Channels with Different Ribs, in: "2010 Int. Conf. Comput. Des. Appl." (ICCDA 2010).

[12] Eiamsa-ard S., Promvonge P., Numerical Study on Heat Transfer of Turbulent Channel Flow Over Periodic Grooves, *Int. Commun. Heat Mass Trans.*, **35**(7):844–852 (2008).

[13] Maiga S.E.B., Nguyen C.T., Galanis N., Roy G., Mare T., Coqueux M., Heat Transfer Enhancement in Turbulent Tube Flow Using Al$_2$O$_3$ Nanoparticle Suspension, *Int. J. Numerical Methods Heat Fluid Flow*, **16**:275-292 (2006).

[14] Palm S.J., Roy G., Nguyen C.T., Heat Transfer Enhancement with the use of Nanofluids in Radial Flow Cooling Systems Considering Temperature Dependent Properties, *Appl. Therm. Eng.*, **26**: 2209-2218 (2006).

[15] Maxwell J.C., "A Treatise on Electricity and Magnetism", Carendon Press, Oxford UK (1873).

[16] Choi S.U.S., Eastman J.A., Enhancing Thermal Conductivity of Cluids with Nano-Particles, "ASME Int. Mech. Eng. Cong. Expo. ", November 12-17, San Francisco, CA (1995).

[17] Eastman J.A., Phillipot S.R., Choi S.U.S., Keblinski P., Thermal Transport in Nanofluids, *Annu. Rev. Mater. Res.*, **34**:219-246 (2004).

[18] Cheng L. Nanofluid Heat Transfer Technologies, *Recent Pat. Eng.,* **3**:1-7 (2009).

[19] Ahamed J.U., Saidur R., Masjuki H.H., A Review on Exergy Analysis of Vapour Compression Refrigeration System, *Renew. Sustain. Energy Rev.*, **15**:1593-1600 (2011).

[20] Keblinski P., Phillpot S.R., Choi S.U.S., Eastman J.A., Mechanisms of Heat Flow in Suspensions of Nano-Sized Particles (Nanofluid), *Int. J. Heat Mass Trans.*, **45**:855-863 (2002).

[21] Das S., Putra N., Thiesen P., Roetzel W. Temperature Dependence of Thermal Conductivity Enhancement for Nanofluids, *J. Heat Trans.,* **125**: 567-574 (2003).

[22] Wang X.Q., Mujumdar A.S., Heat Transfer Characteristics of Nanofluids: A Review, *Int. J. Therm. Sci.*, **46**:1-19 (2007).

[23] Kakaç S., Özerinç S., Yazıcıoğlu A.G., Enhanced Thermal Conductivity of Nanofluids: A State-of-the-Art Review, *Microfluid Nanofluid*, **8**:145-170 (2010).

[24] Jafari A., Shahmohammadi A., Mousavi S.M., CFD Investigation of Gravitational Sedimentation Effect on Heat Transfer of a Nano-Ferrofluid, *Iran. J. Chem. Chem. Eng. (IJCCE)*, **34**(1): 87-96 (2015).

[25] Heris S.Z., Esfahany M.N., Etemad G., Investigation of CuO/water Nanofluid Laminar Convective Heat Transfer Through A Circular tube, *J. Enhanced Heat Trans.*, **13**:279-289 (2006).

[26] Pak B.C., Cho Y.I., Hydrodynamic and Heat Transfer Study of Dispersed Fluids with Submicron Metallic Oxide Particles, *Exp. Heat Trans.*, **11**(2):151–170 (1998).

[27] Xuan Y.M., Li Q., Investigation on Convective Heat Transfer and Flow Features of Nanofluids, *J. Heat Trans.*, **125**:151-155 (2003).

[28] Duangthongsuk W., Wongwises S., Heat Transfer Enhancement and Pressure Drop Characteristics of TiO$_2$/Water Nanofluid in a Double-Tube Counter Flow Heat Exchanger, *Int. J. Heat Mass Trans.*, **52**:2059-2067 (2009).

[29] Fotukian S.M., Nasr Esfahany M., Experimental Study of Turbulent Convective Heat Transfer and Pressure Drop of Dilute CuO/Water Nanofluid Inside A Circular Tube, *Int. Commun. Heat Mass Trans.*, **37**:214-219 (2010).

[30] Wongcharee K., Eiamsa-ard S., Heat Transfer Enhancement by Using CuO/Water Nanofluid in Corrugated Tube Equipped with Twisted Tape, *Int. Commun. Heat Mass Trans.*, **39** (2):251-257 (2012).

[31] Manca O., Nardini S., Ricci D., A Numerical Study of Nanofluid Forced Convection in Ribbed Channels, *Appl. Therm. Eng.*, **37**:280-292 (2012).

[32] Vatani A., Mohammed H.A., Turbulent Nanofluid Flow Over Periodic Rib-Grooved Channels, *Eng. Appl. Comput. Fluid Mech.*, **7**(3):369-381 (2013).

[33] Bejan A., "Entropy Generation Minimization Entropy Generation Minimization: The Method of Thermodynamic Optimization of Finite-Size Systems and Finite-Time Processes", CRC Press, Boca Taron (1995).

[34] Xuan Y., Roetzel W., Conceptions for Heat Transfer Correlation of Nanofluids, *Int. J. Heat Mass Trans.*, **43**:3701–3707 (2000).

[35] Corcione M., Empirical Correlating Equations for Predicting the Effective Thermal Conductivity and Dynamic Viscosity of Nanofluids, *Energy Conv. Manag.*, **52**:789-793 (2011).

[36] Chon C.H., Kihm K.D., Lee S.P., Choi S.U.S., Empirical Correlation Finding the Role of Temperature and Particle Size for Nanofluid (Al$_2$O$_3$) Thermal Conductivity Enhancement, *Appl. Phys. Lett.*, **87**(15): 153107 (2005).

[37] White F.M., "Viscous Fluid Flow", 3rd ed., McGraw Hill, New York, (2006).

[38] www.US-Nano.com.

[39] Bayat J., Nikseresht A.H., Thermal Performance and Pressure Drop Analysis of Nanofluids in Turbulent Forced Convection Flows, *Int. J. Therm. Sci.*, **60**:236-243 (2012).

[40] Rafee R., Rahimzadeh H., Performance Evaluation of a Curved Type Vane Separator at Different Plate Spacings in the Range of 25 to 35mm Using Numerical Simulation, *Iran. J. Chem. Chem. Eng. (IJCCE)*, **29**(3):95-108 (2010).

[41] Eckert E.R.G., Drake R.M., "Heat and Mass Transfer", McGraw-Hill, New York, (1959).

[42] Holman J.P., "Heat Transfer", 9th ed.,McGraw-Hill, New York, 2002.

[43] Cengel Y.A., Ghajar A.F., "Heat and Mass Transfer: Fundamentals and Applications", 4th ed., McGraw-Hill, New York, (2010).

[44] Haaland S.E., Simple and Explicit Formulas for the Friction-Factor in Turbulent Pipe Flow, *Trans. ASME, J. Fluid Eng.*, **105**:89-90 (1973).